# Biomechanical investigation of a passive upper-extremity exoskeleton for manual material handling – a computational parameter study and modelling approach

Bo Eitel Seiferheld

Department of Health Science and Technology,
Aalborg University,
Fredrik Bajers Vej 7D, 9220 Aalborg East, Denmark
and
Department of Materials and Production,
Aalborg University,
Fibigerstræde 16, 9220 Aalborg East, Denmark
Email: bes@mp.aau.dk

Jeppe Frost and Mathias Krog

Department of Health Science and Technology,
Aalborg University,
Fredrik Bajers Vej 7D, 9220 Aalborg East, Denmark
Email: jeppae@rm.dk
Email: math49066@gmail.com

Sebastian Skals

Department of Health Science and Technology,
Aalborg University,
Fredrik Bajers Vej 7D, 9220 Aalborg East, Denmark
and
Musculoskeletal Disorders and Physical Workload,
National Research Centre for the Working Environment,
Lersø Parkallé 105, 2100 Copenhagen East, Denmark
Email: sls@nfa.dk

Michael Skipper Andersen*

Department of Materials and Production,
Aalborg University,
Fibigerstræde 16, 9220 Aalborg East, Denmark
Email: msa@mp.aau.dk
*Corresponding author

**Abstract:** Passive upper-extremity exoskeletons may decrease the risk of developing work-related musculoskeletal disorders. This study examined how shoulder muscle forces and biomechanical loads in the glenohumeral and L4-L5 joint changed as different support torque (1.1 Nm–11.2 Nm) and angle settings (60°–120°) of an exoskeleton were simulated during an overhead manual material handling task. Full-body kinematics of 15 grocery workers, who lifted a bread case (7.9 kg) onto shopping shelves (145.5 cm), were captured on site. The kinematic data were used to drive a detailed human-exoskeleton model based on inverse dynamics. Generally, simulations with maximum torque combined with a peak angle setting between 75°–105° reduced L4-L5 compression and anteroposterior shear forces, glenohumeral contact forces and shoulder flexor muscle forces. The exoskeleton therefore, seemed effective for reducing physical exposure during overhead handling. However, maximum torque with the lowest angle setting, 60°, increased musculoskeletal loading, suggesting that not adjusting the exoskeleton properly could be detrimental.

**Keywords:** musculoskeletal modelling; musculoskeletal diseases; exoskeleton device; lifting; manual material handling; MMH; computer simulation; biomechanics.

**Reference** to this paper should be made as follows: Seiferheld, B.E., Frost, J., Krog, M., Skals, S. and Andersen, M.S. (2022) 'Biomechanical investigation of a passive upper-extremity exoskeleton for manual material handling – a computational parameter study and modelling approach', *Int. J. Human Factors Modelling and Simulation*, Vol. 7, Nos. 3/4, pp.275–300.

**Biographical notes:** Bo Eitel Seiferheld obtained his Bachelor of Science in Sports Science in 2018 from the Aalborg University, Denmark. He obtained his Master of Science degree in Sports Technology, that was completed in 2020 with the specialisation on Biomechanical Exposure and Loading of Exoskeletons at the Department of Health Science and Technology, Aalborg University, Denmark. His research is in the multidisciplinary area between engineering and health science. Here, he develops musculoskeletal models to investigate how the musculoskeletal system responds to biomechanical exposure. He is currently conducting research at the Biomechanical Research Group at the Department of Materials and Production, Aalborg University, Denmark.

Jeppe Frost obtained his Bachelor of Science in Sports Science in 2018. He obtained his Master of Science in Sports Technology in 2020 with the specialisation on Biomechanical Exposure and Loading of Exoskeletons at the Department of Health Science and Technology, Aalborg University, Denmark. His main research interest concerns adapting specific scientific research into meaningful adoptions in occupational settings, through complex interventions. He is currently researching passive upper-extremity exoskeletons in Danish slaughterhouses as a research assistant at the Department of Occupational Medicine, Herning Hospital, Denmark.

Mathias Krog obtained his Bachelor of Science in Sports Science in 2018 from the Aalborg University, Denmark. In 2020, he completed his Master of Science in Sports Technology with the specialisation on Biomechanical Exposure and Loading of Exoskeletons at the Aalborg University, Denmark, at the Department of Health Science and Technology. His interest is within data analysis and data science, where he is currently specialising within machine learning, artificial intelligence, and data science.

Sebastian Skals is a postdoctoral researcher at the National Research Centre for the Working Environment in Copenhagen, Denmark. He obtained his PhD from the Doctoral School in Biomedical Science and Engineering at the Aalborg University, Denmark in 2021. His main areas of research are biomechanics, ergonomics and musculoskeletal modelling with a particular focus on the interplay between physical work factors and musculoskeletal disorders.

Michael Skipper Andersen received his Master of Science in Electrical Engineering with specialisation in Intelligent Autonomous Systems from the Aalborg University in 2004. In 2009, he obtained his PhD from the Department of Mechanical Engineering, Aalborg University, Denmark. Following a short period as Software Engineer in the AnyBody Technology, Aalborg, Denmark, he was employed as an Assistant Professor from 2009–2012 and later in his current position as Associate Professor at the Department of Materials and Production, Aalborg University, Denmark, with both positions being associated with the Biomechanical Research Group. His research is in the multidisciplinary area between engineering and health science, where he develop and apply engineering principles to study health-related issues, primarily in orthopaedics with the ultimate goal to improve patient treatment. He has received several awards for his research and has published more than 70 papers in peer-reviewed international journals and 130 conference abstracts and proceedings.

This paper is a revised and expanded version of a paper entitled 'Biomechanical investigation of a passive upper extremity exoskeleton for manual material handling – a computational parameter study' presented at the 12th Annual Meeting of the Danish Society of Biomechanics, The Department of Health Science and Technology, Sport Sciences-Performance and Technology, Aalborg University, Online, 13 November 2020.

## 1 Introduction

Manual material handling (MMH) refers to the process of moving an item manually by lifting, lowering or carrying them. This process is very common within many occupational settings, as for instance, construction, transportation and retail (Heran-Le Roy et al., 1999). Previous studies have reported strong evidence for the association between work-related musculoskeletal disorders (WMSDs) and MMH tasks (Mayer et al., 2012). In addition, repetitive motions, awkward postures, and/or high forces in the shoulders and back are well-documented risk factors for developing WMSDs (Griffith et al., 2012; van Rijn et al., 2010). Grocery work is an occupation with a high prevalence of WMSDs, with shoulder and lower back disorders accounting for approximately 40% (Anton and Weeks, 2016).

Occupational exoskeletons are emerging as ergonomic tools to assist various workplaces and provide opportunities for improved working conditions, production capabilities and injury prevention (Butler, 2016). Exoskeletons are defined as wearable mechanical structures that enhance the physical capacity of a person. Passive exoskeletons comprise springs designed to aid different body joints by storing and releasing energy, while an active exoskeleton comprises actuators that adds mechanical energy to the system (de Looze et al., 2016).

A variety of passive upper-extremity exoskeletons (PUEXO) are commercially available. Laboratory studies have been fairly consistent in demonstrating reduced shoulder flexor muscle activity during shoulder and overhead drilling (Kim et al., 2018a; Van Engelhoven et al., 2019), overhead tool manipulation (Alabdulkarim et al., 2019; Huysamen et al., 2018; Rashedi et al., 2014), and MMH tasks (Theurel et al., 2018) independent of exoskeleton design. Field testing found similar benefits during cab assembly, frame welding and parts painting (Gillette and Stephenson, 2019, 2018), and worker endurance and productivity were positively affected during boat sanding operations (Moyon et al., 2018) and car assembly (Spada et al., 2018) with a PUEXO.

Even though studies point towards a beneficial effect, firms should act with caution, as negative consequences might also be present. For example, altered kinematics has been observed using two different PUEXO, the PAEXO (Maurice et al., 2020) and the EXHAUSS Stronger® (Theurel et al., 2018), and these changes could result in detrimental humerus and scapula movements (Grieve and Dickerson, 2008). Besides altered kinematics, adjusting the output on the ShoulderX exoskeleton resulted in interference with shoulder antagonist and agonist muscle synergy (Van Engelhoven et al., 2019). Apart from shoulder muscle activities, the erector spinae and internal oblique muscles were observed to be heavily recruited as a consequence of carrying the additional mass from the Steadicam Fawcett Exovest compared to a control condition (Weston et al., 2018). Moreover, undesired load transfer was also found for the aforementioned exoskeleton with increased peak and mean spinal compression and anteroposterior shear forces at the L4-L5 joint (Weston et al., 2018). In contrast, reduced spinal loading was found during heavy and light-weighted drilling, while increased lateral shear was observed during a wiring task with the EksoVest (Kim et al., 2018b). It is obvious that the effects of a PUEXO are highly dependent on the exoskeleton design. Therefore, researchers should focus on determining how to fit an exoskeleton to specific tasks. Finding an optimal solution for specific tasks may act as a catalyst for the product developer to improve the human exoskeleton interaction (Wolf and Wartzack, 2018).

As PUEXO are most often implemented to alleviate the loading on the muscles and joints, a potential approach to task-specific design could be to investigate how internal body quantities in the shoulder and lower back can be minimised by applying different support settings. Internal loads, such as muscle and joint reaction forces (JRFs), are difficult to measure in vivo and require extensive invasive procedures (Bergmann et al., 2007; Wilke et al., 2001, 1999). However, musculoskeletal models can be used to estimate muscle and JRFs based on measurements of kinematics and external forces (Larsen et al., 2020). Furthermore, advancements in inertial measurement unit (IMU)-based motion capture systems has enabled the acquisition of this kinematic input data outside a laboratory environment. Larsen et al. (2020) demonstrated how using this technology in tandem with musculoskeletal modelling could be a useful tool to estimate loadings during MMH tasks with reasonable accuracy.

Therefore, we wanted to design a method to evaluate the effects on musculoskeletal loading associated with using an exoskeleton based on inertial motion capture data obtained in the field. To do this, a human-exoskeletal model was created, comprising both the exoskeleton (commercially available ShoulderX_v3 www.suitx.com) and the human body. Using the human-exoskeleton model, a parameter simulation study was performed, where exoskeleton torque amplitude and torque angle setting (i.e., the angles where torque is provided) from the ShoulderX (Van Engelhoven and Kazerooni, 2019)

were manipulated to identify the optimal solution for reducing musculoskeletal loading during a MMH task.

## 2 Methods

### *2.1 Subjects*

A total of 15 healthy adults (7 men and 8 women, age: 26.3 ± 8.0 years, height: 174.0 ± 7.7 cm, weight: 74.1 ± 13.3 kg, experience: 7.6 ± 5.5 years), full-time employees at two supermarket stores were included in this study. All subjects provided written informed consent before data collection commenced. The study followed the guidelines of The North Denmark Region Committee on Health Research Ethics.

### *2.2 Experimental data*

This study was a part of a larger project aimed at determining the biomechanical loads, muscular demands and working postures during MMH in the Danish supermarket sector (Skals et al., 2021b, 2021a). From this dataset, a two-handed lifting task, where a box of rye bread (7.9 kg) was lifted from a starting position of 15 cm above ground level to a shelf height of approximately 145.5 cm (Figure 1), was chosen for the exoskeleton evaluation. This MMH task was selected as it was deemed relevant for PUEXO work in terms of working height, which required arm elevation at or above shoulder height. During the task, subjects had bilateral peak and mean shoulder flexion angels of 104.8° ± 12.1° and 63.2° ± 11.5° with abduction angles of 65.4° ± 9° and 40.3° ± 6.7°, respectively. Further details on the joint kinematics can be found in an online database (Skals et al., 2020).

**Figure 1** The MMH task that was selected for the evaluation (see online version for colours)

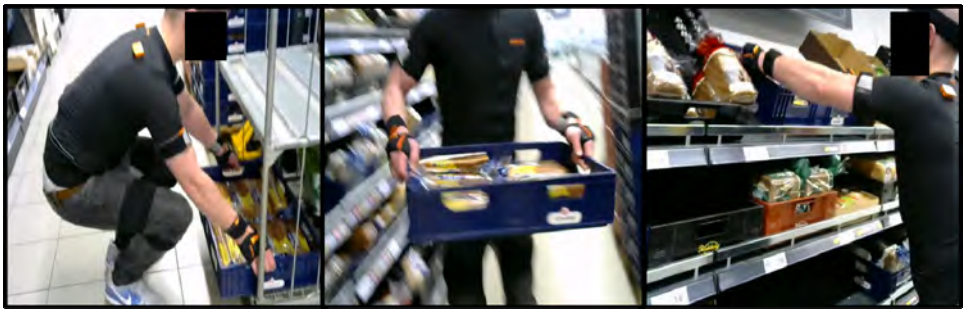

Each subject performed a total of four trials from which full-body kinematic data were captured with an IMU-based motion capture system, the Xsens MVN Awinda wireless motion tracker (Xsens Technologies BV, Enschede, The Netherlands), sampling at 60 Hz. The time series for each trial spanned from the initiation of the lift until the instant the box was placed on the shelf. IMU sensors were attached to the subjects on seventeen body segments: head, sternum, shoulders, upper arms, lower arms, hands, pelvis, thighs, shanks and each foot, according to the user manual. The data from the IMUs were used to

drive a 23-segment kinematic model, which was later used as kinematic input to the musculoskeletal model (see Subsection 2.5).

### *2.3 Exoskeleton*

The commercially available ShoulderX_V3 (SuitX, USA) PUEXO, weighing 3.2 kg, was used in the study. The exoskeleton has adjustable torso height, shoulder width, and arm length, to accommodate user anthropometrics (Figure 2).

**Figure 2** Illustration of the wearable assistive device (ShoulderX_v3) components (see online version for colours)

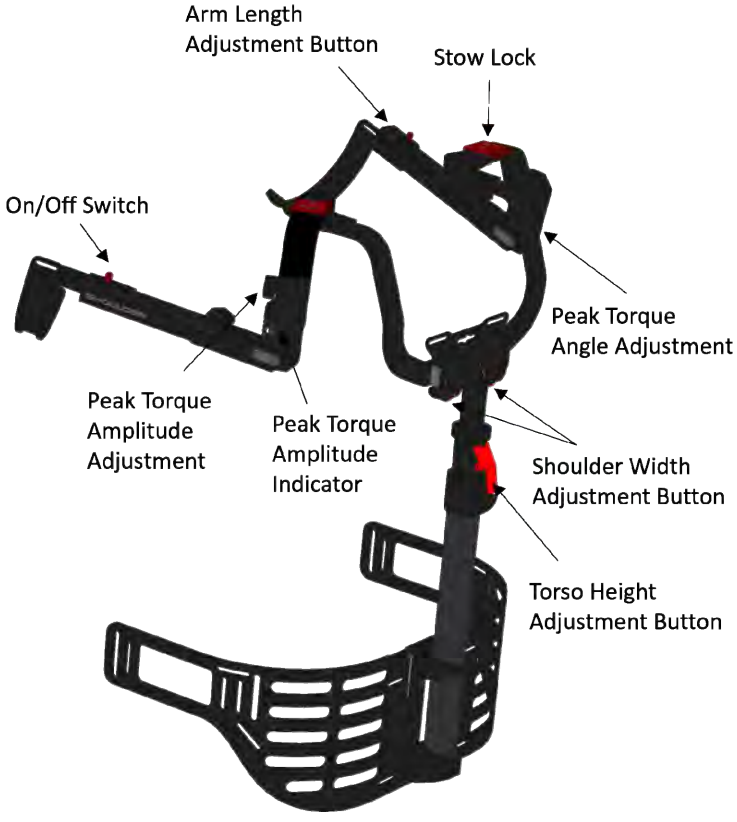


The concept of the ShoulderX is to apply force to the operator's upper arm to unload the shoulder complex and spine by redistributing a fraction of the external load through the exoskeleton structure to the larger muscle groups at the hips and torso (Van Engelhoven and Kazerooni, 2019). The exoskeleton consists of a spring proximal to each glenohumeral joint, providing a passive support when arm elevation occurs. The exoskeleton includes settings to control the support by allowing changes to the arm elevation angles at which the torque occurs and the torque amplitudes themselves (Table 1). When the subject is standing in a neutral posture with the arms positioned alongside the body, it corresponds to an elevation angle of 0° in the revolute joint of the exoskeleton arm.

**Table 1** A summary of torque angle (TA) and torque amplitude settings (TAS) used to adjust the torque profile

| | *Torque angle setting [°]* | | | | | *Torque amplitude setting [Nm]* | | | | |
|---|---|---|---|---|---|---|---|---|---|---|
| | *60* | *75* | *90* | *105* | *120* | *1* | *2* | *3* | *4* | *5* |
| Torque engagement | –10 | 5 | 20 | 35 | 50 | 1.1 | 1.4 | 1.6 | 1.9 | 2.2 |
| Torque peak | 60 | 75 | 90 | 105 | 120 | 5.5 | 6.8 | 8.2 | 9.7 | 11.2 |
| Torque disengagement | 100 | 115 | 130 | 145 | 160 | 3.2 | 3.8 | 4.3 | 4.9 | 5.5 |

Notes: A 0° angle corresponding to the arms placed in a neutral position alongside the body. Note that italic text emphasises the different settings that were used on the exoskeleton.

The exoskeleton has adjustment options within the upper and lower boundaries of these settings, where each combination results in a specific torque profile. For example, setting '90°, 3' results in the output shown in Figure 3(a). Thus, a profile of the torque output can be created for each combination of settings (Figure 3).

**Figure 3** (a) Single torque profile response as a function of elevation angle at the discrete setting '90°, 3' (b) Torque profile response to three different discrete torque amplitude settings as a function of elevation angle at '90°, 5' (blue), '90°, 3' (black), and '90°, 1' (red) (c) Torque profile response to three different discrete torque angle settings as a function of elevation angle '60°, 3' (green), '90°, 3' (black), and '120°, 3' (magenta) (see online version for colours)

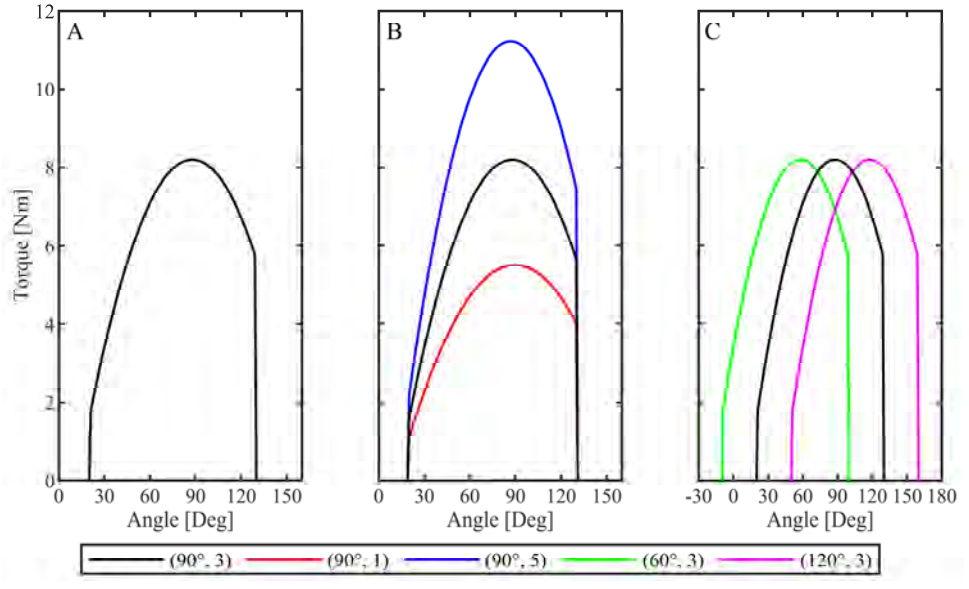


## *2.4 Building the model*

Full-body kinematic data were processed and used to drive a detailed computer model co-simulating the human, exoskeleton and box using inverse dynamics. The model was composed of a musculoskeletal human body (i.e., bones, joints, and muscles), a box

representing the carried goods, and an exoskeleton model (i.e., mechanical components, joints, and passive elastic elements). These models were connected to form a single mechanical system. The detailed human-exoskeletal model was built in the AnyBody Modelling System v.7.2 (AMS) (AnyBody Technology A/S, Aalborg, Denmark). An overview of the process is depicted in Figure 4. We briefly describe this model in Figure 4, but otherwise focus on describing the model additions for the present study.

**Figure 4** Flowchart showing the steps from experimental data collection to the development of the human-exoskeleton model in the AMS and the setup of the computational parameter variation with simulations of the different torque profiles for the manual material handling task (see online version for colours)

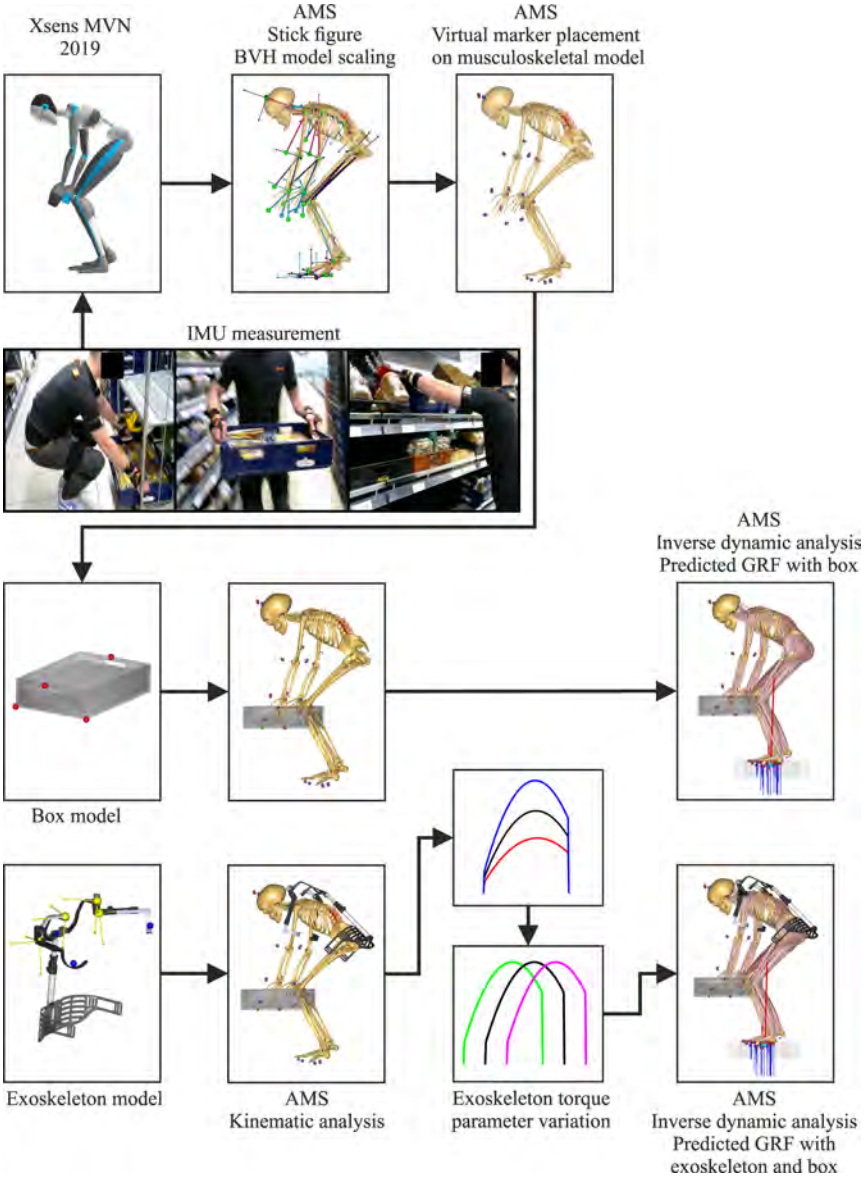

### *2.5 Musculoskeletal model*

The musculoskeletal model was based on the BVH_XSENS model template from the AnyBody Managed Model Repository (AMMR) v.2.2.3, which includes a method for predicting ground reaction forces and moments (Karatsidis et al., 2019). The generic human musculoskeletal model was comprised of a lower extremity model (Carbone et al., 2015), thoracolumbar and cervical spine models (de Zee et al., 2007; Han et al., 2012; Hansen et al., 2006), and a shoulder and arm model (Van der Helm et al., 1992; Veeger et al., 1997, 1991). Further details can be found in the AMMR documentation (Lund et al., 2021).

#### *2.5.1 Model scaling and kinematic analysis*

The recorded motion capture data were exported from the Xsens MVN Analyze software and imported as a stick figure model into the AMS. Hereafter, the musculoskeletal model was scaled based on the joint-to-joint distances from the stick figure model using a linear scaling law. The Xsens stick figure contains 72 DOF, whereas the musculoskeletal model in the AMS contains 44 DOF. Due to this incompatibility, a virtual marker tracking method was used (Karatsidis et al., 2019), where virtual markers were attached to both the stick figure and musculoskeletal model and the least-square difference between these were minimised to resolve the musculoskeletal model kinematics (Andersen et al., 2009).

#### *2.5.2 Exoskeleton and box models*

A 3D computer-aided design (CAD) model of the handled merchandise was created in SolidWorks v. 2017.5.0 (Dassault Systems, Vélizy-Villacoublay Cedex, France) and subsequently imported into the AMS. The geometry, mass and inertial properties were taken from measurements during data collection and a cuboid with the material properties of the merchandise was modelled and placed inside a shell with the properties of cardboard. Likewise, a 3D CAD model of the ShoulderX exoskeleton was created using SolidWorks v. 2019.0. The digital exoskeleton was adjusted to each subject according to the settings recommended in the fitting guidelines (i.e., torso height, shoulder width and arm length), using measured anthropometrics from the collected data. The subject-specific exoskeleton model that was imported into the AMS had 10 DOF. The hip brace had six DOF and each arm had two revolute joints, thus four DOF in total. The revolute joint that followed the motion in the transversal plane were located superior to the glenohumeral joint centre, a few centimetres above the acromion (cf. Figure 5). The last revolute joint followed the motion in both the sagittal and frontal plane depending on the position of the revolute joint in the transversal plane. This joint is positioned on the lateral side of the glenohumeral joint, and the assistive torque was provided in this joint.

#### *2.5.3 Kinematic analysis of the box and exoskeleton*

To form the human-exoskeletal model, the exoskeleton and box had to be kinematically connected to the musculoskeletal model. Here, the exoskeleton and box were superimposed onto the kinematics derived from the initial analysis of the MMH task and constrained based on reference nodes and coordinate systems created on both the exoskeleton, box and human models. This process was separated into two different

kinematic analyses: one solving the musculoskeletal model with hand-box interaction and subsequently one solving the human-exoskeleton interaction. The kinematic analysis was separated to avoid artificially induced differences between the musculoskeletal model tracking the experimental data and the over-determinate connection to the exoskeleton. Firstly, the movement of the musculoskeletal model were determined by tracking the stick figure data and, subsequently, the exoskeleton was attached to the musculoskeletal model to ensure that the musculoskeletal kinematics remained unchanged. For both analyses, we used a combination of soft and hard constraints and applied the nonlinear least-squares optimisation algorithm to minimise the least-square errors on the soft constraints while satisfying the hard constraints (Andersen et al., 2009).

**Figure 5** Node representation of the nodes on the box (red), exoskeleton (blue) and musculoskeletal model (green) (see online version for colours)

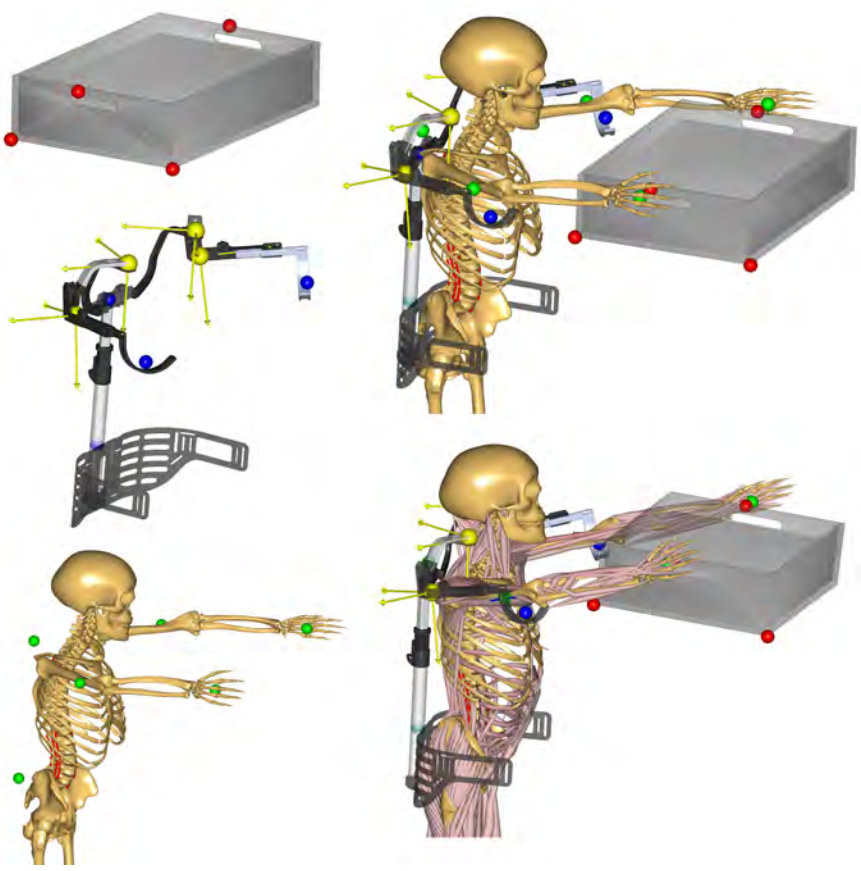

Notes: Yellow nodes and coordinate systems represents the two revolute joints on the exoskeleton. Note that the corresponding coordinate systems for the box, exoskeleton and musculoskeletal model were omitted for clarity.

For the hand-box interaction, soft constraints between a point in the middle of the hand and on the handle of the box were created. Additionally, to prevent rotation of the box in the sagittal plane, a reference node was placed at the right proximal and distal corner of the box to ensure that the two notes always remained the same distance above the ground

(Figure 5). This constraint was created to control the box rotation along its longitudinal axis, as this DOF was not determined by the constraints with the hands. The box was still allowed to rotate in the frontal and transversal plane according to the motion of the hands. This constraint was justified based on video observations of the participants that showed little rotation of the box in the sagittal plane.

For the human-exoskeleton interaction, reference nodes were placed at the sacrum and at the hip brace of the exoskeleton, where hard constraints were created in all translational directions and around the vertical axis with soft constraints around the transverse and sagittal rotational axis. A reference node was implemented proximal to C7 and on the exoskeleton frame by the shoulder width adjustment and connected by a hard constraint to track forward and backward bending. Lastly, reference nodes were placed bilaterally above the elbow joint on the humerus and at the support point of the exoskeleton arm brace. Hard constraints were created in the mediolateral and anteroposterior directions, while soft constraints were defined for the rotational directions to allow the humerus to rotate inside the arm brace (Figure 5).

### *2.5.4 Kinetics – prediction of external forces*

To simulate the different torque profiles that the PUEXO can provide, a 2nd order polynomial fit was implemented into the AMS to replicate the torque profiles of the exoskeleton (Van Engelhoven and Kazerooni, 2019) as a function of the angles that were captured in the exoskeleton arms from the kinematic analysis. Thus, the discrete values from Table 1 were used to calculate the continuous values of the supportive torque that was provided during the task (Figure 3). Control conditions were implemented to ensure that the torque was only provided within the engagement and disengagement angles.

Unidirectional contact elements were implemented to model the force transmission between the ground, exoskeleton, box and musculoskeletal model. Rather than conventional force plate measurements, the ground reaction forces and moments (GRF&M) were predicted. This method has shown similar accuracy to that of force plates during various activities (Fluit et al., 2014; Karatsidis et al., 2019; Skals et al., 2017). The method utilises 25 dynamic contact elements distributed under each foot of the musculoskeletal model. Each dynamic contact element consists of five uniaxial force actuators, which can generate a normal force in addition to positive and negative static friction forces in the anteroposterior- and mediolateral directions (Fluit et al., 2014). These forces are constrained by a nonlinear strength function, which ensures that forces can only be generated when the nodes are close to the ground and almost stationary (Skals et al., 2017). Between the hands and box as well as the humerus and exoskeleton arm brace, 24 unidirectional contact elements were inserted and made part of the muscle recruitment problem (see below). These contact elements were implemented to resolve the indeterminacy of the closed chains created by the interaction with the exoskeleton and box and were modelled with very high strength (400,000 N). The high strength was chosen to ensure that the contact elements, even when generating forces, would contribute minimally to the objective function and enable the model to recruit these forces if they were beneficial to reduce the muscular load. The contact elements between the hands and box allowed for force transfer in all directions, with force components subdivided into positive and negative directions, resulting in 12 unidirectional force actuators for each hand-box interaction (six related to forces and six related to moments). With respect to the human-exoskeleton contact elements, some assumptions regarding

their interaction were made. For the contact between the humerus and exoskeleton arm brace, only translational uniaxial reaction forces were generated in the sagittal and mediolateral direction, thus disregarding potential friction forces along the longitudinal axis to the arm. In a real-life scenario, some friction forces would be expected. In total, this resulted in four force actuators for each humerus and exoskeleton arm brace contact element. Three reaction forces and three reaction moments were introduced between the sacrum and exoskeleton hip brace.

In addition to the contact elements, small residual forces and torques with a strength of 10 N and 10 Nm were applied to the pelvis. The actuation of the contact elements was solved as part of the muscle recruitment along with the muscle and residual forces [equation (1)].

## *2.6 Muscle recruitment*

The AMS is based on an inverse dynamics approach, where motion and applied forces are input and used to compute the unknown forces (e.g., joint torques, joint reaction and muscle forces) based on the dynamic equilibrium equations and assumptions about how the central nervous system solves the muscle recruitment problem. From the information of inertial properties, mass, orientation, location, size and connections of the human model, the box, and the exoskeleton, an inverse dynamics analysis was performed fundamentally based on the Newton-Euler equations (Damsgaard et al., 2006). However, because the musculoskeletal system contains many more actuators (i.e., muscles) than DOF and because of the formed closed chains, these equilibrium equations are indeterminate. Therefore, computing the muscle recruitment response and hereby, determining the unknown forces, without knowing the specific recruitment pattern from the central nervous system is impossible. To overcome this issue, an optimisation problem was setup to minimise muscle forces, while fulfilling the equilibrium equations and ensuring that the muscles can only pull (Damsgaard et al., 2006). In practice, this means that the forces between the exoskeleton and human, box and hands, and feet and ground were incorporated as part of the muscle recruitment optimisation problem:

$$\underset{\mathrm{f}}{\text{minimise}}\, G\left(\mathrm{f}^{(\mathrm{M})}, \mathrm{f}^{(\mathrm{K})}, \mathrm{f}^{(\mathrm{R})}\right) = \sum_{i=1}^{n^{(\mathrm{M})}} \left(\frac{f_i^{(\mathrm{M})}}{N_i^{(\mathrm{M})}}\right)^3 + \sum_{i=1}^{n^{(\mathrm{K})}} \left(\frac{f_i^{(\mathrm{K})}}{N_i^{(\mathrm{K})}}\right)^3 + \sum_{i=1}^{n^{(\mathrm{R})}} \left(\frac{f_i^{(\mathrm{R})}}{N_i^{(\mathrm{R})}}\right)^3 \quad (1)$$

$$n^{(K)} = 5n^{(C)} + 12n^{(H)} + 4n^{(E)} \quad (2)$$

$$f_i^{(K)} = \begin{bmatrix} f_i^{(C)^T} & f_i^{(H)^T} & f_i^{(E)^T} \end{bmatrix}^T \quad (3)$$

$$\text{Subject to } \mathbf{Cf} = \mathbf{d} \quad (4)$$

$$0 \leq f_i^{(\mathrm{M})},\ i = 1, \ldots, n^{(\mathrm{M})}, \quad (5)$$

$$0 \leq f_i^{(\mathrm{K})},\ i = 1, \ldots, n^{(\mathrm{K})}, \quad (6)$$

$$0 \leq f_i^{(\mathrm{R})},\ i = 1, \ldots, n^{(\mathrm{R})}. \quad (7)$$

where $G$ is the objective function, representing the criterion of muscle recruitment from the central nervous system as a function of all unknown forces $f$, i.e., muscle forces, $f^{(\mathrm{M})}$,

contact element forces, $f^{(K)}$, and residual forces $f^{(R)}$. $n^{(M)}$ is the number of muscles, $f_i^{(M)}$, the force of the $i^{th}$ muscle, $N_i^{(M)}$ is the strength of the $i^{th}$ muscle. $n^{(K)}$ is the total number of contact elements for the predicted GRFs, $5n^{(C)}$, hand and box, $12n^{(H)}$, and exoskeleton and humerus, $4n^{(E)}$. $f_i^{(K)}$ is a vector that contains the $i^{th}$ GRF, $f_i^{(C)}$, $i^{th}$ force between hand and box, $f_i^{(H)}$, and $i^{th}$ force between exoskeleton and humerus, $f_i^{(E)}$. $N_i^{(K)}$ is the strength of the $i^{th}$ contact element. $n^{(R)}$ is the number of residual forces and moments on the pelvis, $f_i^{(R)}$ is the $i^{th}$ residual force and $N_i^{(R)}$ is the strength of the residual force. The objective function $G$ is subjected to $\mathbf{Cf} = \mathbf{d}$, where $\mathbf{C}$ is the coefficient matrix for the dynamic equilibrium equations, while the vector $\mathbf{f}$ includes the unknown muscle, joint reaction, contact and residual forces, and $\mathbf{d}$ contains all known applied loads and inertia forces [equation (4)]. The non-negativity constraints state that all contact forces can only be positive [equations (5)–(7)]. Please notice that the JRFs within the anatomical joints of the human and the joints within the exoskeleton are not included in the objective function but are only in the equilibrium equations (4). The contact element forces, $f^{(K)}$, relate only to the contacts between the human and the external elements, i.e., the box, exoskeleton and ground.

### *2.7 Parameter variation and computation*

Due to the purpose of finding the optimal exoskeleton setting that minimised spinal and shoulder joint reaction and muscular forces during grocery stocking, a parameter study was performed by varying the torque angle and amplitude settings of the exoskeleton (Table 1). Additionally, simulations of the MMH task were performed without the exoskeleton and with the exoskeleton equipped, but not activated. All these combinations led to a total of 27 configurations × 1 task × 4 trials × 15 subjects being simulated in AMS resulting in 1.620 simulations.

### *2.8 Data analysis*

Dependent measures consisted of peak and impulse muscular, 3D spine and shoulder forces. Muscle forces were estimated for the shoulder agonists muscles, including the anterior deltoid (AD), middle deltoid (MD), and upper trapezius (UT). Similarly, the posterior deltoid (PD), latissimus dorsi (LD), and teres major (TMA) were included as antagonist muscles. Supraspinatus (SS), infraspinatus (IS), teres minor (TMI), and subscapularis (SC) were included to represent stabilising forces to the rotator cuff. In AMS, every muscle is subdivided into several parts, wrapping around specific joints. For simplification, the muscle part with the highest peak force was included for further analysis. For the spine, L4–L5 superoinferior compression ($F_{comp}^{L4\text{-}L5}$), anteroposterior shear ($F_{AP}^{L4\text{-}L5}$), and mediolateral shear ($F_{ML}^{L4\text{-}L5}$) forces were extracted. For the shoulder, glenohumeral contact force (*GHCF*) as well as glenohumeral superoinferior ($R_{SI}$) and anteroposterior shear ($R_{AP}$) ratio to compression ($R_{COMP}$) impulse and peak force were estimated (Klemt et al., 2018). All peak forces were normalised to percentage of body weight (%BW) and impulse to %BW per second (%BW × s). For every dependent variable, a 3D fine grid was created plotting the dependent measurement with the torque angle and amplitude setting of the exoskeleton.

## 3 Results

Generally, simulations with the exoskeleton equipped with no active torque increased the JRFs overall when compared to no exoskeleton. L4-L5 compression and shear peak forces as well as compression impulse were decreased as the exoskeleton was simulated in an active setting (Figure 6). The JRFs were uniformly decreasing with the additional torque, but changing the angles appeared to both reduce and increase reaction forces. An optimum between the simulated variables were observed at setting '90°, 5'. Mediolateral shear forces were omitted as these were considered negligible (<2%BW).

**Figure 6** L4–L5 impulse and peak values of, (a) compression (b) anteroposterior shear forces normalised to body weight as a function of variations in the torque amplitude settings (TAS) and torque angle settings (TA) (see online version for colours)

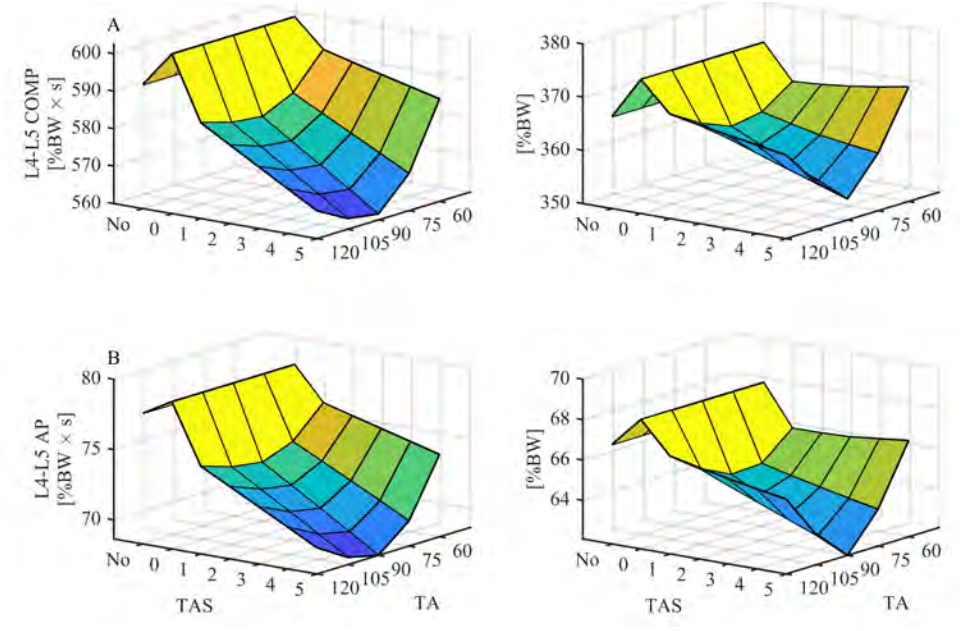


Notes: TAS of 0, 1, 2, 3, 4 and 5 corresponded to a peak torque of 0, 5.5, 6.8, 8.2, 9.7, 11.2 Nm, respectively, while TA of 60, 75, 90, 105, 120 corresponded to the peak angles in degrees with torque engaging at 70 degrees below peak and disengaging at 40 degrees above peak. 'No' indicates performing the task without the exoskeleton.

The GHCFs had a more complicated pattern than the L4–L5 JRFs. Here, simulations with peak torque at 60° resulted in additional impulse and peak forces independently of torque output [Figure 7(a)]. Whenever the simulations were performed with peak torques at and above 75°, the GHCFs would decrease below that of working without an exoskeleton. The highest reductions of GHCFs were obtained once the exoskeleton was simulated at setting '105°, 5' for both the impulse and peak values. The anteroposterior shear to compression ratio in the glenohumeral joint was reduced whenever the exoskeleton was simulated with an active torque profile. The exoskeleton was most beneficial when operating with torque profiles at '90°, 5' and '75°, 5' with absolute changes of 0.10 and 0.07 when ratios were computed from the impulse and peak values, respectively

[Figure 7(b)]. The ratio of superoinferior shear impulse to compression impulse showed reductions. However, the ratio of superoinferior peak shear to peak compression increased: for example, at setting '60°, 5' the ratio had a relative change of 35% and went from 0.23 to 0.34 [Figure 7(c)].

**Figure 7** Glenohumeral impulse and peak values for the, (a) contact force (b) anteroposterior ratio (c) superoinferior ratio normalised to body weight as a function of variations in the torque amplitude settings (TAS) and torque angle settings (TA) (see online version for colours)

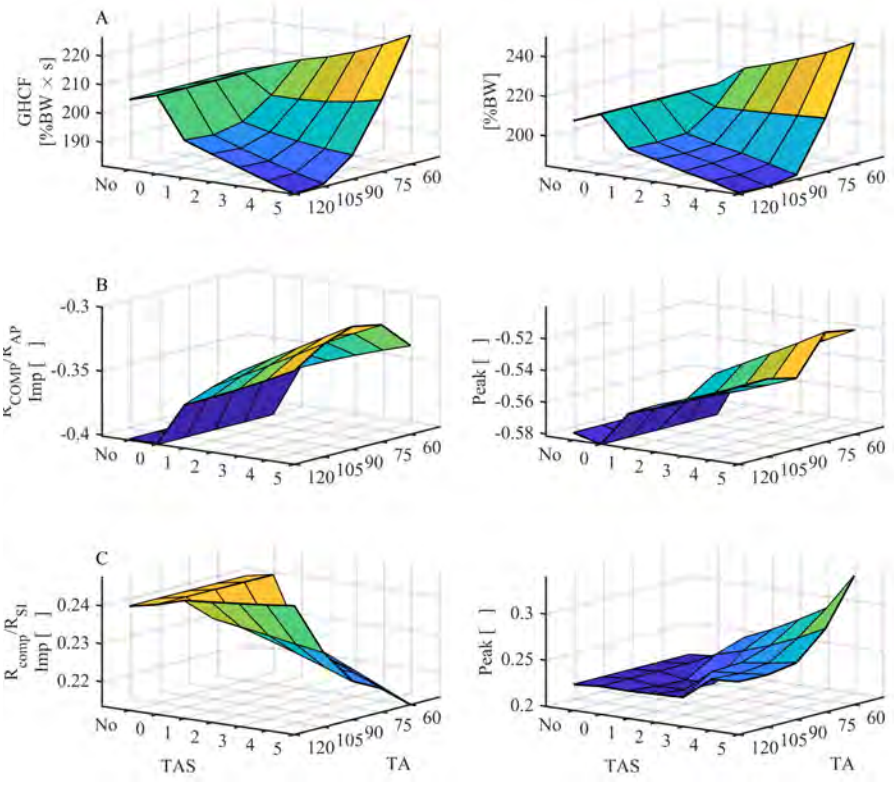


Notes: TAS of 0, 1, 2, 3, 4 and 5 corresponded to a peak torque of 0, 5.5, 6.8, 8.2, 9.7, 11.2 Nm, respectively, while TA of 60, 75, 90, 105, 120 corresponded to the peak angles in degrees with torque engaging at 70 degrees below peak and disengaging at 40 degrees above peak. 'No' indicates performing the task without the exoskeleton.

The simulations clearly indicated that agonist muscle impulse was reduced as additional torque was added to the upper arms. Peak forces showed the same tendency once the angle was adjusted at and above 75° (Figure 8). Agonist muscles showed absolute reductions ranging from 4–7.3%BW × s and 4–6.2%BW for impulse and peak, respectively, when comparing the best setting '105°, 5' with no exoskeleton. These absolute reductions corresponded to a percentage reduction ranging between 31%–46% for impulse and 23–32% for peak. On the other hand, antagonist muscles showed a reversed tendency. LD and TMA muscle forces were uniformly increasing with additional torque, while decreasing the angles resulted in higher forces for both impulse

and peak values at setting ‘60°, 5’ [Figures 9(b)–9(c)]. Thus, performing the MMH task without the exoskeleton seemed to be preferable to reduce antagonist muscle forces. However, PD showed the same tendency as for the agonist muscles.

**Figure 8** Shoulder agonist muscle forces with impulse and peak values for, (a) anterior deltoid (b) middle deltoid (c) upper trapezius normalised to body weight as a function of variations in the 28 torque amplitude settings (TAS) and torque angle settings (TA) (see online version for colours)

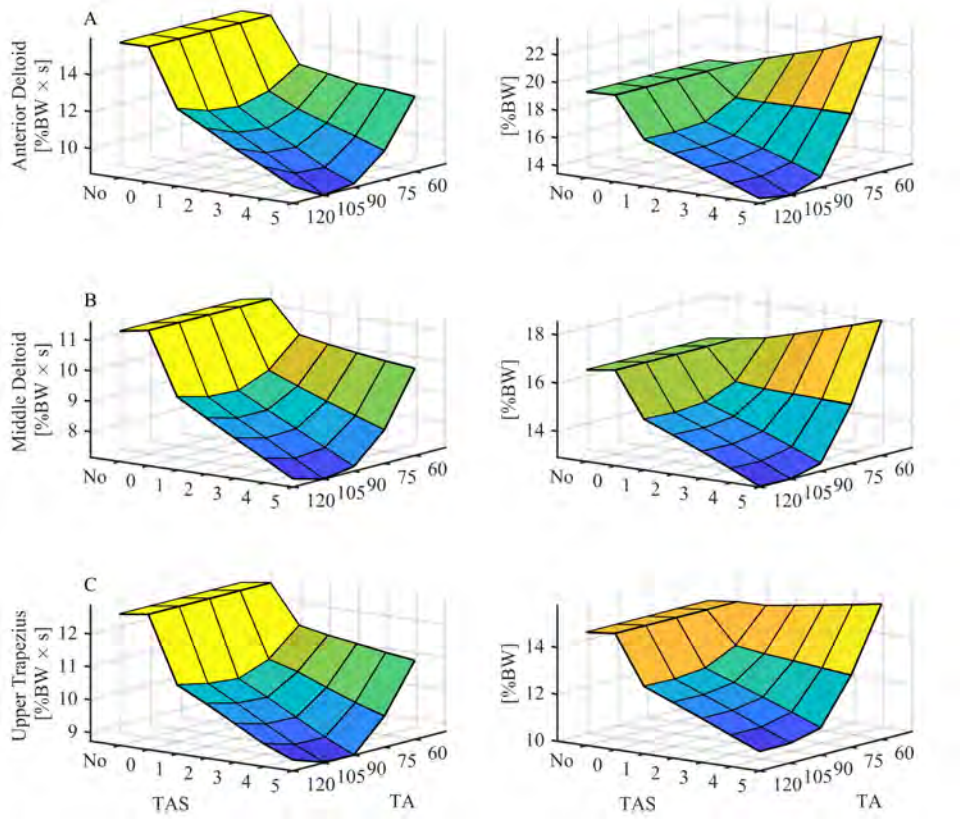


Notes: TAS of 0, 1, 2, 3, 4 and 5 corresponded to a peak torque of 0, 5.5, 6.8, 8.2, 9.7, 11.2 Nm, respectively, while TA of 60, 75, 90, 105, 120 corresponded to the peak angles in degrees with torque engaging at 70 degrees below peak and disengaging at 40 degrees above peak. ‘No’ indicates performing the task without the exoskeleton.

Overall, rotator cuff muscle forces increased when subjects were simulated with the exoskeleton (Figure 10), especially infraspinatus, with up to 32% and 23.5% relative changes for impulse and peak, respectively, compared with no exoskeleton [Figure 10(a)]. Independent of rotator cuff muscle the highest forces were observed at exoskeleton setting ‘60°, 5’. At this setting rotator cuff muscles increased and had a relative average change of 24.3% for impulse and 47% for peak values compared to not wearing an exoskeleton during the task (please note supraspinatus was excluded as it was hardly activated). Thus, the optimal solution to reduce rotator cuff muscle forces was to perform the MMH without an exoskeleton.

**Figure 9** Shoulder antagonist muscle forces with impulse and peak values for, (a) posterior deltoid (b), latissimus dorsi (c) teres major normalised to body weight as a function of variations in the torque amplitude settings (TAS) and torque angle settings (TA) (see online version for colours)

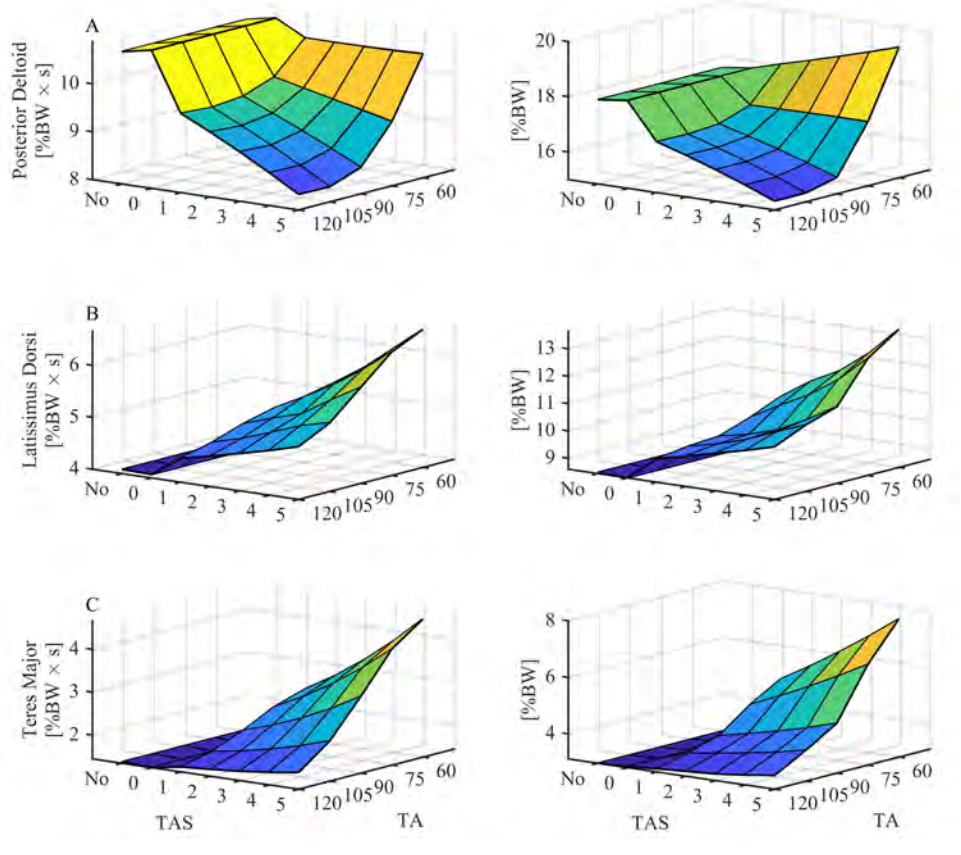


Notes: TAS of 0, 1, 2, 3, 4 and 5 corresponded to a peak torque of 0, 5.5, 6.8, 8.2, 9.7, 11.2 Nm, respectively, while TA of 60, 75, 90, 105, 120 corresponded to the peak angles in degrees with torque engaging at 70 degrees below peak and disengaging at 40 degrees above peak. 'No' indicates performing the task without the exoskeleton.

## 4 Discussion

We evaluated the musculoskeletal loading associated with using an exoskeleton for assistance when performing a MMH task in two grocery stores. In doing so, a detailed human-exoskeletal model based on inverse dynamics was developed and driven using kinematic data from an IMU-based motion capture system. We ran a computational parameter study on the human-exoskeletal model to identify how variations of the support torque amplitude and angle settings of the exoskeleton affected joint reaction and muscle forces. Simulations of these various settings revealed that working with the PUEXO could have both positive and negative effects on musculoskeletal loading.

Especially settings with maximum torque combined with a peak support angle between 75–105° were found to be beneficial for reducing musculoskeletal load. Contrarily, maximum torque combined with a peak support angle of 60° exposed the musculoskeletal system to additional loading beyond what was experienced without the exoskeleton. Thus, adjusting the settings correctly is imperative for the protective effects of the device.

**Figure 10** Rotator cuff muscle forces with impulse and peak values for, (a) infraspinatus (b) teres minor (c) subscapularis normalised to body weight as a function of variations in the torque amplitude settings (TAS) and torque angle settings (TA) (see online version for colours)

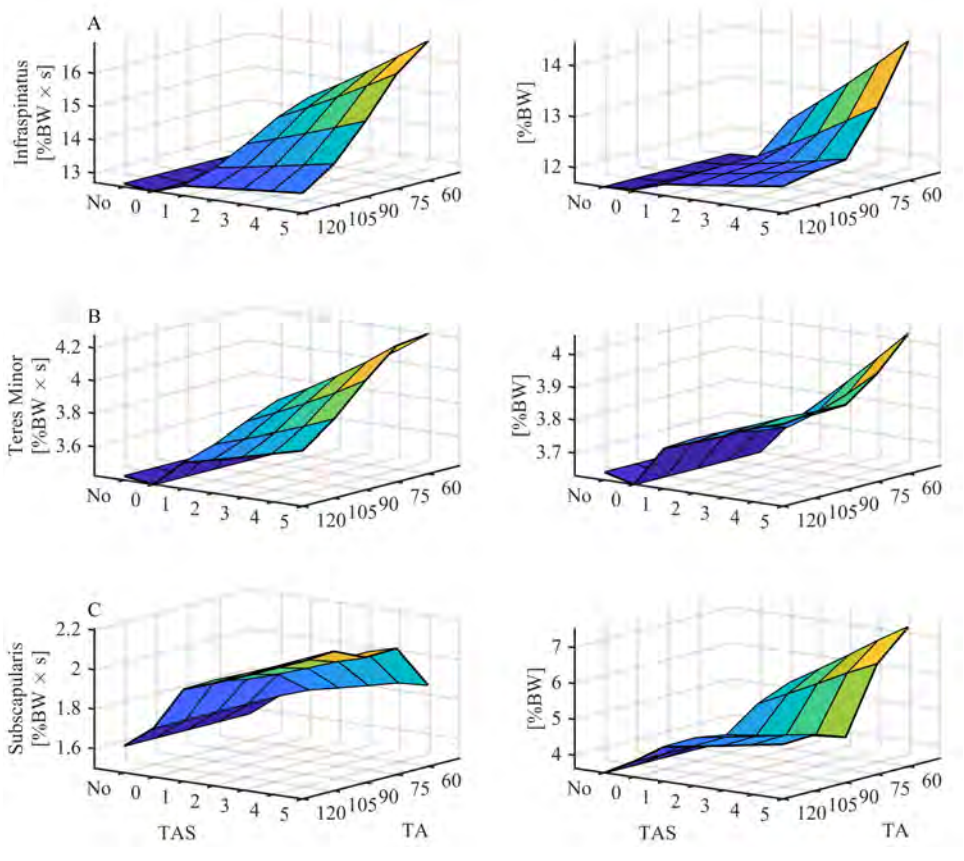


Notes: TAS of 0, 1, 2, 3, 4 and 5 corresponded to a peak torque of 0, 5.5, 6.8, 8.2, 9.7, 11.2 Nm, respectively, while TA of 60, 75, 90, 105, 120 corresponded to the peak angles in degrees with torque engaging at 70 degrees below peak and disengaging at 40 degrees above peak. 'No' indicates performing the task without the exoskeleton.

Generally, the idea behind occupational exoskeletons is to redirect forces from sensitive to sturdier joints (Theurel and Desbrosses, 2019). From our results, it was clear that the ShoulderX device was capable of shifting the loads, as evidenced by reduced spinal and shoulder forces. The instance of peak joint loading during the lifting cycle was either at pick up or when placing the box on the shelf, which was similar to performing the task

without the exoskeleton (Skals et al., 2021a). The JRFs were commonly uniformly decreasing with additional torque, but changing the angles exhibited a nonlinear behaviour with both reduced and increased loadings (cf. Figures 6–8). For the spine, notable reductions were observed when the angle was changed from 60° to 75°, while the effect seemingly plateaued in the range of 75–105° before additional loads were observed when changed from 105° to 120°. The shoulder forces showed similar tendencies, but an angle of 60° increased the loading beyond what was experienced without the exoskeleton. Therefore, using the exoskeleton at the upper and lower boundaries (i.e., 120 and 60°) were less protective compared to angles between (75–105°) for the investigated MMH task. Thus, it is important that the torque provided by the exoskeleton match the torque provided by the muscles during the movement to ensure a protective effect of the device.

For the lumbar spine, tolerance limits of 3,400 N for compression and 1,000 N for shear has been suggested for infrequent lifting (Gallagher and Marras, 2012; Waters et al., 1993). If loads on the spinal column exceed the tolerance limits, the likelihood of mechanical damage to the spinal structures is expected to increase (Marras, 2012). For the average subject simulated (74.1 kg), the compression and shear forces would peak at 367%BW (≈2,670 N) and 67%BW (≈490 N) without wearing an exoskeleton, where the most effective exoskeleton setting would reduce this to 354%BW (≈2,575 N) and 62%BW (≈450 N). In both cases, the forces would not exceed the defined tolerance limits. However, it is important to address that being within these limits is not necessarily concomitant with no biomechanical risk, as fatigue failure of the tissues are the prevailing cause of damage (Gallagher and Marras, 2012). Contrary to our findings, increased spinal loads (Weston et al., 2018), paraspinal muscle activity and perceived discomfort (Rashedi et al., 2014) were observed with a non-anthropomorphic PUEXO with a mechanical arm. Discrepancies may have been a result of the additional mass and a larger torque about the lower back caused by the mechanical arm operating along an axis separate from the operator's upper extremities. The ShoulderX has an anthropomorphic frame configuration and this type of design may indirectly assist users in maintaining better trunk posture and spinal stability, as suggested with a similar PUEXO (Kim et al., 2018a). Lastly, a secondary analysis of back kinetics indicated that while performing the MMH task, the forces in the erector spinae muscles were reduced. For example, the peak forces in the erector spinae longissimus thoracic and multifidi were reduced with up to 13% and 5%, respectively, when comparing unassisted lifting with the exoskeleton setting '90°, 5'. It is conceivable that the reduced muscle forces in the back may be reflected in the L4-L5 compression and shear JRFs as the overall effort of the musculoskeletal system was alleviated by the assistance provided by the exoskeleton.

The GHCF when handling the box without the exoskeleton was on average 209%BW, while using the exoskeleton at the most ineffective and effective setting resulted in GHCFs of 246%BW and 184%BW, respectively. In comparison, a previous study showed average GHCFs of 180%BW and 240%BW for two-handed lifting of a 5 kg box to shoulder height and a lateral movement of a 10 kg suitcase (Anglin et al., 2000), respectively. Their results corresponded well with our estimations of GHCFs when lifting a 7.9 kg rye bread box without assistance. Nevertheless, GHCFs were almost three times higher than common daily activities (Bergmann et al., 2007; Klemt et al., 2018), suggesting that the MMH task was a relatively strenuous activity. Investigating only GHCFs may lead to information loss, as the ratio between shear force to compression may help determine the risk for shoulder injuries (Klemt et al., 2018).

Compression forces keep the humeral head within the glenoid socket, while shear forces contribute to destabilisation by translating the humeral head towards the glenoid rim (Klemt et al., 2018). The musculoskeletal model in the AMS works in a similar way with the humeral head constrained inside the glenoid. However, the model does not allow for shoulder dislocation, thus giving no direct measurement of instability in terms of displacement within the glenoid. Instead, the model calculates the glenohumeral JRFs necessary to keep the humeral head from dislocating, where a reduced compression force and increased shear force are indicative of instability (Vidt et al., 2018). Our results suggested that reducing glenohumeral joint luxation was complicated, as different torque profiles led to varying results [cf. Figures 7(b) and 7(c)]. Thus, choosing a setting that reduced both shoulder and spinal loading was challenging, as no optimal solution was found. Nevertheless, our results suggest it is more likely that the total demand of the shoulder and spinal complex were reduced with the exoskeleton evidenced by our results. However, to elucidate dislocation risks further, JRFs relative to the edge of the glenoid could be investigated, as has been done for the hip previously (Mellon et al., 2013), but this was beyond the scope of this study.

Increasing the torque amplitude at appropriate angles was associated with reduced shoulder muscle forces in UT, AD, MD and PD with relative changes up to 45% for both impulse and peak forces, compared with no exoskeleton (Figure 8). Previous research have shown similar relative changes for the peak and median muscle activities of the same muscles using the ShoulderX device (Van Engelhoven et al., 2019) and a similar PUEXO (Alabdulkarim et al., 2019; Gillette and Stephenson, 2019; Kim et al., 2018a). In contrast, LD and TMA exhibited a reverse change resulting in higher muscle forces when wearing the exoskeleton. This is in accordance with previous results showing the same tendency for the extensor muscle activity with the same device for a small percentage of their subjects (Van Engelhoven et al., 2019). Besides superficial muscles, deeper muscles in the rotator cuff were investigated. Rotator cuff muscles stabilise the glenohumeral joint by compressing the humeral head into the glenoid, where interference may alter the loads on the joint (Parsons et al., 2002). As GHCF changed with different torque profiles, the musculoskeletal model had to respond appropriately by recruiting muscles to maintain shoulder stability and prevent shoulder dislocation. This is especially apparent at setting ‘60°, 5’, where the highest GHCFs were observed. Thus, it is possible that IS and TMI were recruited to maintain shoulder stability [cf. Figure 7(a) with Figures 9(b) and 9(c)]. As GHCFs dropped below the forces observed when performing the MMH without an exoskeleton, rotator cuff forces also decreased. However, the rotator cuff forces were still higher then performing the task without the exoskeleton, potentially due to the reduced forces observed in the larger shoulder muscles (i.e., deltoideus and UT). Drawing such a conclusion seems reasonable since external rotation of the humerus is the primary function of the IS and TMI, i.e., to help stabilise the humeral head and prevent it from sliding out of the glenoid (Terry and Chopp, 2000). In addition, the increased activation could be due to the imposed forces of the exoskeleton arms, which produces undesirable forces in the anterior or lateral directions. Instead of assisting the lift at lower angles, it pushes the humeral head in an anterior direction away from the glenoid. Thus, IS and TMI muscle forces must be recruited to stabilise the shoulder, during medial rotation, to prevent anterior dislocation of the humerus.

In general, matching an optimal torque profile to the task is essential for correct exoskeleton use, but as shown, the effects on musculoskeletal loading changes with various settings, sometimes increasing the loads. Thus, choosing the ideal setting that

would accommodate both the spinal and shoulder complex can be a challenging process. Nevertheless, our findings suggest that a PUEXO could potentially be used to reduce musculoskeletal loading and hereby, decrease the risks of WMSDs. However, the scope of exoskeletons expands beyond worker safety and well-being, as it also encompasses productivity optimisation (McFarland and Fischer, 2019; Spada et al., 2018) with an economically-driven incentive. As demonstrated in previous research, worker endurance and productivity can be positively affected during various tasks at manufacturing firms with an exoskeleton (Moyon et al., 2018; Spada et al., 2019, 2018). If the use of an exoskeleton effectively reduces task demands, while simultaneously increasing the workers' endurance and productivity, it might incentivise companies to increase the frequency of the task and hereby, potentially eliminate the beneficial effects of the exoskeleton. This is an important aspect to consider when implementing exoskeletons in industrial settings.

### *4.1 Limitations*

The present study has several limitations that should be noted. Musculoskeletal models based on inverse dynamics are derived from kinematics and measured or estimated external forces. IMU-based motion capture systems are less accurate than optical motion capture systems (Larsen et al., 2020), which was particularly apparent for the most distal segments in the present study, particularly the hand position. Additionally, inaccuracies might occur during the virtual marker tracking, as this method attempts to find a compromise between both kinematic models (Andersen et al., 2009). Additionally, the kinematics of the PUEXO and box was predicted entirely from the movements of the musculoskeletal model. Measuring the motion with the subjects wearing the PUEXO would improve the quality of the model, as studies suggest that wearing an exoskeleton could interfere with natural movement (Maurice et al., 2020; Theurel et al., 2018). However, the performed parameter study on the variation of exoskeleton settings would have been very comprehensive to conduct experimentally and could have risked excessively fatiguing the subjects. In addition to the limitations related to the motion capture procedures, we did also not attempt to evaluate the simulation results using experimental data, such as electromyographic (EMG) measurements. By incorporating EMG, we could have measured the activities of the surface musculature and evaluated whether the simulation results showed similar activation patterns. However, this would have necessitated repeating these measurements for each torque/angle setting, hereby removing the advantageous of performing a simulation-based parameter study. Furthermore, performing all these additional lifts would have increased the influence of muscular fatigue, which would inhibit this evaluation to some extent.

Correct modelling of the contact elements (human-box, human-exoskeleton, and human-ground) plays a crucial role in the force transmission between the human body and external objects. Even though the humerus was allowed to slide within the exoskeleton arm brace during the kinematic analysis, these uniaxial reaction forces, resulting in friction forces, were omitted. Implementing the generated friction forces would enhance the model and enable a more realistic simulation of the interaction between the segments. Moreover, reaction moments were assumed to be small and without any impact as the exoskeleton arm mechanism supposedly allowed for free rotation. Disregarding these forces, and any other possible points of force transfer,

compromises the accuracy of the simulated estimations to some extent and could be implemented to enhance the model's estimations.

## 5 Conclusions

In summary, a state-of-the-art musculoskeletal model was developed to analyse how different exoskeleton torque profiles altered the dynamic loading of the spine and shoulders during an overhead MMH task using IMU-based kinematic data obtained at two supermarkets. Generally, 3D spine and shoulder JRFs were reduced when the exoskeleton was adjusted to the supposedly best settings compared to lifting without the exoskeleton. Shoulder agonist muscle forces were also reduced with the exoskeleton, but additional demands were observed for the shoulder antagonists and rotator cuff muscles. Selecting the optimal exoskeleton setting that minimise the overall musculoskeletal load was challenging as both positive and negative effects were observed. Thus, our findings suggest that workplaces should act cautiously when implementing exoskeletons, as inappropriate use could lead to an increased risk of WMSDs. However, our findings suggest that a carefully planned implementation strategy could reduce musculoskeletal loading and possibly reduce the risk to the workers.

## Acknowledgements

A special thanks to SuitX for providing us with the necessary CAD model and information of the ShoulderX exoskeleton. We would also like to thank the volunteers for their participation.

## References

Alabdulkarim, S., Kim, S. and Nussbaum, M.A. (2019) 'Effects of exoskeleton design and precision requirements on physical demands and quality in a simulated overhead drilling task', *Appl. Ergon.*, Vol. 80, pp.136–145 [online] https://doi.org/10.1016/j.apergo.2019.05.014.

Andersen, M.S., Damsgaard, M. and Rasmussen, J. (2009) 'Kinematic analysis of over-determinate biomechanical systems', *Comput. Methods Biomech. Biomed. Engin.*, Vol. 12, pp.371–384 [online] https://doi.org/10.1080/10255840802459412.

Anglin, C., Wyss, U.P. and Pichora, D.R. (2000) 'Glenohumeral contact forces', *Proc. Inst. Mech. Eng. Part H J. Eng. Med.*, Vol. 214, pp.637–644 [online] https://doi.org/10.1243/0954411001535660.

Anton, D. and Weeks, D.L. (2016) 'Prevalence of work-related musculoskeletal symptoms among grocery workers', *Int. J. Ind. Ergon.*, Vol. 54, pp.139–145 [online] https://doi.org/10.1016/j.ergon.2016.05.006.

Bergmann, G., Graichen, F., Bender, A., Kääb, M., Rohlmann, A. and Westerhoff, P. (2007) 'In vivo glenohumeral contact forces – measurements in the first patient 7 months postoperatively', *J. Biomech.*. Vol. 40, pp.2139–2149 [online] https://doi.org/10.1016/j.jbiomech.2006.10.037.

Butler, T.R. (2016) 'Exoskeleton technology: making workers safer and more productive', *Prof. Saf.*, Vol. 61, pp.32–36.

Carbone, V., Fluit, R., Pellikaan, P., van der Krogt, M.M., Janssen, D., Damsgaard, M., Vigneron, L., Feilkas, T., Koopman, H.F.J.M. and Verdonschot, N. (2015) 'TLEM 2.0 – a comprehensive musculoskeletal geometry dataset for subject-specific modeling of lower extremity', *J. Biomech.*, Vol. 48, pp.734–741 [online] https://doi.org/10.1016/j.jbiomech.2014.12.034.

Damsgaard, M., Rasmussen, J., Christensen, S.T., Surma, E. and de Zee, M. (2006) 'Analysis of musculoskeletal systems in the AnyBody Modeling System', *Simul. Model. Pract. Theory*, Vol. 14, pp.1100–1111 [online] https://doi.org/10.1016/j.simpat.2006.09.001.

de Looze, M.P., Bosch, T., Krause, F., Stadler, K.S. and O'Sullivan, L.W. (2016) 'Exoskeletons for industrial application and their potential effects on physical work load', *Ergonomics*, Vol. 59, pp.671–681 [online] https://doi.org/10.1080/00140139.2015.1081988.

de Zee, M., Hansen, L., Wong, C., Rasmussen, J. and Simonsen, E.B. (2007) 'A generic detailed rigid-body lumbar spine model', *J. Biomech.*, Vol. 40, pp.1219–1227 [online] https://doi.org/10.1016/j.jbiomech.2006.05.030.

Fluit, R., Andersen, M.S., Kolk, S., Verdonschot, N. and Koopman, H.F.J.M. (2014) 'Prediction of ground reaction forces and moments during various activities of daily living', *J. Biomech.*, Vol. 47, pp.2321–2329 [online] https://doi.org/10.1016/j.jbiomech.2014.04.030.

Gallagher, S. and Marras, W.S. (2012) 'Tolerance of the lumbar spine to shear: a review and recommended exposure limits', *Clin. Biomech.*, Vol. 27, pp.973–978 [online] https://doi.org/10.1016/j.clinbiomech.2012.08.009.

Gillette, J.C. and Stephenson, M.L. (2018) 'EMG analysis of an upper body exoskeleton during automotive assembly', *Proc. 42nd Annu. Meet. Am. Soc. Biomech.*, pp.308–309.

Gillette, J.C. and Stephenson, M.L. (2019) 'Electromyographic assessment of a shoulder support exoskeleton during on-site job tasks', *IISE Trans. Occup. Ergon. Hum. Factors*, Vol. 7, pp.1–9 [online] https://doi.org/10.1080/24725838.2019.1665596.

Grieve, J.R. and Dickerson, C.R. (2008) 'Overhead work: Identification of evidence-based exposure guidelines', *Occup. Ergon.*, Vol. 8, pp.53–66 [online] https://doi.org/10.3233/OER-2008-8105.

Griffith, L.E., Shannon, H.S., Wells, R.P., Walter, S.D., Cole, D.C., Côté, P., Frank, J., Hogg-Johnson, S. and Langlois, L.E. (2012) 'Individual participant data meta-analysis of mechanical workplace risk factors and low back pain', *Am. J. Public Health*, Vol. 102, pp.309–318 [online] https://doi.org/10.2105/AJPH.2011.300343.

Han, K.S., Zander, T., Taylor, W.R. and Rohlmann, A. (2012) 'An enhanced and validated generic thoraco-lumbar spine model for prediction of muscle forces', *Med. Eng. Phys.*, Vol. 34, pp.709–716 [online] https://doi.org/10.1016/j.medengphy.2011.09.014.

Hansen, L., De Zee, M., Rasmussen, J., Andersen, T.B., Wong, C. and Simonsen, E.B. (2006) 'Anatomy and biomechanics of the back muscles in the lumbar spine with reference to biomechanical modeling', *Spine (Phila. Pa. 1976)*, Vol. 31, pp.1888–1899 [online] https://doi.org/10.1097/01.brs.0000229232.66090.58.

Heran-Le Roy, O., Niedhammer, I., Sandret, N. and Leclerc, A. (1999) 'Manual materials handling and related occupational hazards: a national survey in France', *Int. J. Ind. Ergon.*, Vol. 24, pp.365–377 [online] https://doi.org/10.1016/S0169-8141(99)00004-9.

Huysamen, K., Bosch, T., de Looze, M., Stadler, K.S., Graf, E. and O'Sullivan, L.W. (2018) 'Evaluation of a passive exoskeleton for static upper limb activities', *Appl. Ergon.*, Vol. 70, pp.148–155 [online] https://doi.org/10.1016/j.apergo.2018.02.009.

Karatsidis, A., Jung, M., Schepers, H.M., Bellusci, G., de Zee, M., Veltink, P.H. and Andersen, M.S. (2019) 'Musculoskeletal model-based inverse dynamic analysis under ambulatory conditions using inertial motion capture', *Med. Eng. Phys.*, Vol. 65, pp.68–77 [online] https://doi.org/10.1016/j.medengphy.2018.12.021.

Kim, S., Nussbaum, M.A., Mokhlespour Esfahani, M.I., Alemi, M.M., Alabdulkarim, S. and Rashedi, E. (2018a) 'Assessing the influence of a passive, upper extremity exoskeletal vest for tasks requiring arm elevation: part I – 'expected' effects on discomfort, shoulder muscle

activity, and work task performance', *Appl. Ergon.*, Vol. 70, pp.315–322 [online] https://doi.org/10.1016/j.apergo.2018.02.025.

Kim, S., Nussbaum, M.A., Mokhlespour Esfahani, M.I., Alemi, M.M., Jia, B. and Rashedi, E. (2018b) 'Assessing the influence of a passive, upper extremity exoskeletal vest for tasks requiring arm elevation: part II – 'unexpected' effects on shoulder motion, balance, and spine loading', *Appl. Ergon.*, Vol. 70, pp.323–330 [online] https://doi.org/10.1016/j.apergo.2018.02.024.

Klemt, C., Prinold, J.A., Morgans, S., Smith, S.H.L., Nolte, D., Reilly, P. and Bull, A.M.J. (2018) 'Analysis of shoulder compressive and shear forces during functional activities of daily life', *Clin. Biomech.*, Vol. 54, pp.34–41 [online] https://doi.org/10.1016/j.clinbiomech.2018.03.006.

Larsen, F.G., Svenningsen, F.P., Andersen, M.S., de Zee, M. and Skals, S. (2020) 'Estimation of spinal loading during manual materials handling using inertial motion capture', *Ann. Biomed. Eng.*, Vol. 48, pp.805–821 [online] https://doi.org/10.1007/s10439-019-02409-8.

Lund, M.E., Tørholm, S., Simonsen, S.T. and Engelund, B.K. (2021) 'The AnyBody managed model repository (AMMR)' [online] https://doi.org/10.5281/ZENODO.4616316.

Marras, W.S. (2012) 'The complex spine: The multidimensional system of causal pathways for low-back disorders', *Hum. Factors*, Vol. 54, pp.881–889 [online] https://doi.org/10.1177/0018720812452129.

Maurice, P., Ivaldi, S., Babic, J., Camernik, J., Gorjan, D., Schirrmeister, B., Bornmann, J., Tagliapietra, L., Latella, C., Pucci, D. and Fritzsche, L. (2020) 'Objective and subjective effects of a passive exoskeleton on overhead work', *IEEE Trans. Neural Syst. Rehabil. Eng.*, Vol. 28, pp.152–164 [online] https://doi.org/10.1109/tnsre.2019.2945368.

Mayer, J., Kraus, T. and Ochsmann, E. (2012) 'Longitudinal evidence for the association between work-related physical exposures and neck and/or shoulder complaints: a systematic review', *Int. Arch. Occup. Environ. Health*, Vol. 85, pp.587–603 [online] https://doi.org/10.1007/s00420-011-0701-0.

McFarland, T. and Fischer, S. (2019) 'Considerations for industrial use: a systematic review of the impact of active and passive upper limb exoskeletons on physical exposures', *IISE Trans. Occup. Ergon. Hum. Factors*, Vol. 7, pp.1–26 [online] https://doi.org/10.1080/24725838.2019.1684399.

Mellon, S.J., Grammatopoulos, G., Andersen, M.S., Pegg, E.C., Pandit, H.G., Murray, D.W. and Gill, H.S. (2013) 'Individual motion patterns during gait and sit-to-stand contribute to edge-loading risk in metal-on-metal hip resurfacing', *Proc. Inst. Mech. Eng. Part H J. Eng. Med.*, Vol. 227, pp.799–810 [online] https://doi.org/10.1177/0954411913483639.

Moyon, A., Poirson, E. and Petiot, J.F. (2018) 'Experimental study of the physical impact of a passive exoskeleton on manual sanding operations', *Procedia CIRP*, Vol. 70, pp.284–289 [online] https://doi.org/10.1016/j.procir.2018.04.028.

Parsons, I.M., Apreleva, M., Fu, F.H. and Woo, S.L.Y. (2002) 'The effect of rotator cuff tears on reaction forces at the glenohumeral joint', *J. Orthop. Res.*, Vol. 20, pp.439–446 [online] https://doi.org/10.1016/S0736-0266(01)00137-1.

Rashedi, E., Kim, S., Nussbaum, M.A. and Agnew, M.J. (2014) 'Ergonomic evaluation of a wearable assistive device for overhead work', *Ergonomics*, Vol. 57, pp.1864–1874 [online] https://doi.org/10.1080/00140139.2014.952682.

Skals, S., Bláfoss, R., Andersen, L.L., Andersen, M.S. and de Zee, M. (2021a) 'Manual material handling in the supermarket sector. Part 2: knee, spine and shoulder joint reaction forces', *Appl. Ergon.*, Vol. 92, p.103345 [online] https://doi.org/10.1016/j.apergo.2020.103345.

Skals, S., Bláfoss, R., Andersen, M.S., de Zee, M. and Andersen, L.L. (2021b) 'Manual material handling in the supermarket sector. Part 1: joint angles and muscle activity of trapezius descendens and erector spinae longissimus', *Appl. Ergon.*, Vol. 92, p.103340 [online] https://doi.org/10.1016/j.apergo.2020.103340.

Skals, S., Bláfoss, R., Andersen, L.L., de Zee, M. and Andersen, M.S. (2020) 'Manual material handling in the supermarket sector: full dataset' [online] https://doi.org/10.5281/ZENODO.4312624.

Skals, S., Jung, M.K., Damsgaard, M. and Andersen, M.S. (2017) 'Prediction of ground reaction forces and moments during sports-related movements', *Multibody Syst. Dyn.*, Vol. 39, pp.175–195 [online] https://doi.org/10.1007/s11044-016-9537-4.

Spada, S., Ghibaudo, L., Carnazzo, C., Gastaldi, L. and Cavatorta, M.P. (2019) 'Passive upper limb exoskeletons: an experimental campaign with workers', in Bagnara, S., Tartaglia, R., Albolino, S., Alexander, T. and Fujita, Y. (Eds.): *Advances in Intelligent Systems and Computing*, pp.230–239, Springer International Publishing, Cham [online] https://doi.org/10.1007/978-3-319-96068-5_26.

Spada, S., Ghibaudo, L., Gilotta, S., Gastaldi, L. and Cavatorta, M.P. (2018) 'Analysis of exoskeleton introduction in industrial reality: main issues and EAWS risk assessment', pp.236–244 [online] https://doi.org/10.1007/978-3-319-60825-9_26.

Terry, G.C. and Chopp, T.M. (2000) 'Functional anatomy of the shoulder', *J. Athl. Train.*, Vol. 35, pp.248–255 [online] https://doi.org/10.1093/ptj/46.10.1043.

Theurel, J. and Desbrosses, K. (2019) 'Occupational exoskeletons: overview of their benefits and limitations in preventing work-related musculoskeletal disorders', *IISE Trans. Occup. Ergon. Hum. Factors*, Vol. 7, pp.264–280 [online] https://doi.org/10.1080/24725838.2019.1638331.

Theurel, J., Desbrosses, K., Roux, T. and Savescu, A. (2018) 'Physiological consequences of using an upper limb exoskeleton during manual handling tasks', *Appl. Ergon.*, Vol. 67, pp.211–217 [online] https://doi.org/10.1016/j.apergo.2017.10.008.

Van der Helm, F.C.T., Veeger, H.E.J., Pronk, G.M., Van der Woude, L.H.V. and Rozendal, R.H. (1992) 'Geometry parameters for musculoskeletal modelling of the shoulder system', *J. Biomech.*, Vol. 25, pp.129–144 [online] https://doi.org/10.1016/0021-9290(92)90270-B.

Van Engelhoven, L. and Kazerooni, H. (2019) 'Design and intended use of a passive actuation strategy for a shoulder supporting exoskeleton', *2019 Wearable Robot. Assoc. Conf. WearRAcon 2019*, pp.7–12 [online] https://doi.org/10.1109/WEARRACON.2019.8719402.

Van Engelhoven, L., Poon, N., Kazerooni, H., Rempel, D., Barr, A. and Harris-Adamson, C. (2019) 'Experimental evaluation of a shoulder-support exoskeleton for overhead work: influences of peak torque amplitude, task, and tool mass', *IISE Trans. Occup. Ergon. Hum. Factors*, Vol. 7, pp.1–14 [online] https://doi.org/10.1080/24725838.2019.1637799.

van Rijn, R.M., Huisstede, B.M., Koes, B.W. and Burdorf, A. (2010) 'Associations between work-related factors and specific disorders of the shoulder – a systematic review of the literature', *Scand. J. Work. Environ. Health*, Vol. 36, pp.189–201 [online] https://doi.org/10.5271/sjweh.2895.

Veeger, H.E.J., Van Der Helm, F.C.T., Van Der Woude, L.H.V., Pronk, G.M. and Rozendal, R.H. (1991) 'Inertia and muscle contraction parameters for musculoskeletal modelling of the shoulder mechanism', *J. Biomech.*, Vol. 24, pp.615–629 [online] https://doi.org/10.1016/0021-9290(91)90294-W.

Veeger, H.E.J., Yu, B., An, K-N. and Rozendal, R.H. (1997) 'Parameters for modeling the upper extremity', *J. Biomech.*, Vol. 30, pp.647–652 [online] https://doi.org/10.1016/S0021-9290(97)00011-0.

Vidt, M.E., Santago, A.C., Marsh, A.P., Hegedus, E.J., Tuohy, C.J., Poehling, G.G., Freehill, M.T., Miller, M.E. and Saul, K.R. (2018) 'Modeling a rotator cuff tear: individualized shoulder muscle forces influence glenohumeral joint contact force predictions', *Clin. Biomech.*, Vol. 60, pp.20–29 [online] https://doi.org/10.1016/j.clinbiomech.2018.10.004.

Waters, T.R., Putz-Anderson, V., Garg, A. and Fine, L.J. (1993) 'Revised NIOSH equation for the design and evaluation of manual lifting tasks', *Ergonomics*, Vol. 36, pp.749–776 [online] https://doi.org/10.1080/00140139308967940.

Weston, E.B., Alizadeh, M., Knapik, G.G., Wang, X. and Marras, W.S. (2018) 'Biomechanical evaluation of exoskeleton use on loading of the lumbar spine', *Appl. Ergon.*, Vol. 68, pp.101–108 [online] https://doi.org/10.1016/j.apergo.2017.11.006.

Wilke, H.J., Neef, P., Caimi, M., Hoogland, T. and Claes, L.E. (1999) 'New in vivo measurements of pressures in the intervertebral disc in daily life', *Spine (Phila. Pa. 1976)*, Vol. 24, pp.755–762 [online] https://doi.org/10.1097/00007632-199904150-00005.

Wilke, H-J., Neef, P., Hinz, B., Seidel, H. and Claes, L. (2001) 'Intradiscal pressure together with anthropometric data – a data set for the validation of models', *Clin. Biomech.*, Vol. 16, pp.S111–S126 [online] https://doi.org/10.1016/S0268-0033(00)00103-0.

Wolf, A. and Wartzack, S. (2018) 'Parametric movement synthesis: towards virtual optimisation of man-machine interaction in engineering design', *Proc. Int. Des. Conf. Des.*, Vol. 2, pp.941–952 [online] https://doi.org/10.21278/idc.2018.0400.